Spatial filtering by chirped photonic crystals

V. Purlys,[1] L. Maigyte,[2] D. Gailevičius,[1] M. Peckus,[3] M. Malinauskas,[1] and K. Staliunas[2,4]

[1]*Laser Research Center, Department of Quantum Electronics, Vilnius University, Sauletekio al 10, LT-10222 Vilnius, Lithuania*

[2]*Departament de Física i Enginyeria Nuclear, Universitat Politècnica de Catalunya, Colom 11, 08222 Terrassa, Spain*

[3]*Center for Physical Sciences and Technology, Savanoriu Ave. 231, LT-02300, Vilnius, Lithuania*

[4]*Institució Catalana de Recerca i Estudis Avançats (ICREA), Pg. Lluís Companys, 23, 08010 Barcelona, Spain*

(Received 17 December 2012; published 11 March 2013)

We show, theoretically and experimentally, that chirped photonic crystals (where the longitudinal modulation period varies along the propagation direction) can provide a substantial spatial (angular) filtering of light beams. The chirped photonic crystals, in gapless configuration, were recorded in a bulk of glass, where the refraction index has been periodically modulated using tightly focused femtosecond laser pulses. The spatial filtering performance has been studied in detail, and the filtering efficiencies up to approximately 50% have been experimentally demonstrated.

DOI: 10.1103/PhysRevA.87.033805 PACS number(s): 42.79.−e, 42.25.Fx

I. INTRODUCTION

Spatial filtering is broadly used to improve the spatial quality of light beams. A conventional technique of spatial filtering uses a confocal system of lenses to form a far field image in the focal plane, where a diaphragm of appropriate diameter is positioned in order to remove undesired angular components of the spatial spectrum [1]. Recently, alternative methods of spatial filtering have been proposed, based on light propagation through materials with periodically modulated refractive index on a wavelength scale—the photonic crystals (PhCs).

The PhCs are well known to exhibit photonic band gaps in frequency domain, i.e., the frequency ranges at which light waves cannot propagate [2], therefore they can provide *frequency* filtering, i.e., removing the undesired frequency components of the radiation. In analogy to the frequency band gaps, the *angular* band gaps are also possible in PhCs. If the band gap for a given frequency appears at some angle to the optical axis, so that the on- and around-axis radiation modes are allowed to propagate, then the effect can result in angular low-angle-pass filtering. The spatial filtering in one-dimensional (1D) PhCs is, however, inefficient in praxis, as the positions of the angular band gaps are highly sensitive to the longitudinal modulation period. Instead, the angular filtering has been considered in 1D periodic structures with defect [3], which however work for large angles with respect to direction of index modulation.

The angular positions of angular band gaps is better controllable in two-dimensional (2D) photonic crystals, where the refraction index is modulated in longitudinal as well as in transverse direction. The appearance of the band gaps require the condition on the longitudinal modulation period $d_{||} < \lambda$. Such filtering has been proposed in optics [4–7], also in acoustics, for periodic acoustic media (sonic crystals) [8], and also is recently demonstrated experimentally in acoustics [9]. The mechanism of spatial filtering due to the angular band gaps is illustrated in Figs. 1(a) and 1(b), where the position of the center of the angular band gap follows from geometrical considerations, and corresponds to a resonant interaction between the field harmonic.

Alternatively, the spatial filtering in PhCs without angular band gaps was recently proposed [10]. In the latter case particular angular components of the radiation are not reflected back, but are deflected to the forward direction [see Figs. 1(c) and 1(d) for illustration]. The gapless filtering is possible for longitudinal periods of modulation $d_{||} > \lambda$. First experimental evidences of the gapless spatial filtering have been given in three-dimensional PhCs [11]. The gapless filtering has been also proposed to clean the spatial structure of Bose-Einstein condensates [12].

The fabrication of the gapless spatial filters is more convenient, as not so small longitudinal periods are required. On the other hand, the efficiency of filtering is restricted, as the deflected wave components propagate in forward direction, and can be scattered back into the modes of initial radiation. The process is summarized in Fig. 2, where the gapless filtering depending on the length of nonchirped PhC is shown. (We postpone the description of numeric as well as experiment to the following sections.)

Evident is that initially the "dips" in the angular spectrum (the filtered out angular regions) increase in depth with increasing crystal length (Fig. 2, $n = 8, 14$). However, when the area being filtered is depleted to zero, the reverse process starts, and the efficiency of the filtering starts decreasing (Fig. 2, $n = 20, 22$). Moreover, the filtered out area appears to be not a smooth dip, but develops an oscillatory shape. This is in contrast with the spatial filtering based on the band gaps, where the filtered out radiation propagates in a backward direction, and cannot be scattered back. As a consequence, the filtered out angular areas monotonically increase with the propagation length in PhCs with angular band gaps.

In order to achieve efficient angular filtering the reverse scattering process is to be suppressed, i.e., the interaction between harmonics is to be allowed for a limited propagation distance, and interrupted at the distance before the reverse process starts. For the parameters of Fig. 2, the optimum length providing maximum dip of filtered out components is approximately 14 periods. However, at the optimal distance the filtering dip is of a limited width. Another possibility to increase the efficiency is the use of chirped structures [10], where the longitudinal period varies along the photonic structure. As the filtering angle depends on the longitudinal period of the PhC, the angle sweeps along the chirped structure. As the result one can obtain simultaneously: (1) the

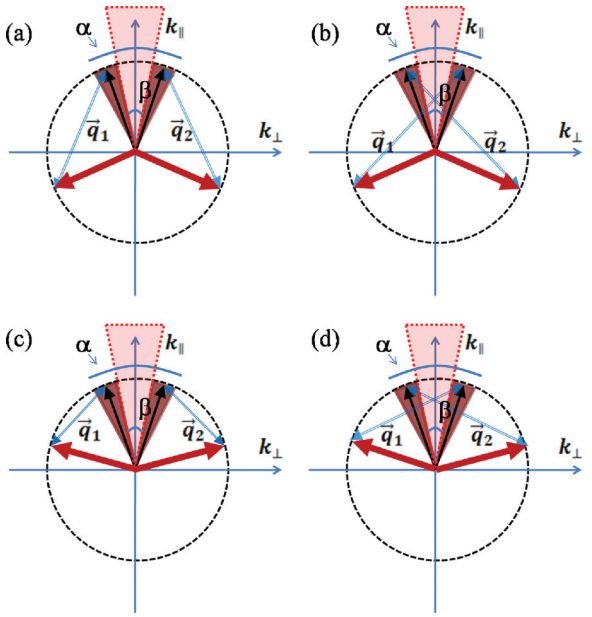

FIG. 1. (Color online) Illustration of spatial filtering in a 2D PhC, in spatial Fourier domain (k_x, k_y) in configuration with (a), (b) and without (c), (d) the angular band gaps. Filtering occurs when the waves in the dark triangle zones get into resonant scattering condition with modulation with wave vectors $\vec{q} = (q_x, q_z)$ (blue arrows). Thick red arrows show the direction of filtered out angular components. The spatial spectrum (far field) of the initial beam, consisting of the central (regular) part, and of the wings (the part to be removed), is shown by bright and dark triangles.

angular range of filtered out components can be increased, i.e., determined by the sweep of the instantaneous filtering angle along the full length of the crystal; and (2) the reverse scattering process can be suppressed, as the efficient interaction length of the angular components is limited by the velocity of the sweep.

The article is devoted to the experimental demonstration of the above described idea, and to the quantitative analysis of the efficiency of the angular filtering in the presence of chirp. Next, in Sec. II we describe the fabrication and measurement of the chirped PhC samples. In following, in Sec. III we describe a numerical scheme allowing us to efficiently calculate the light propagation through the structure. The experimental results and numerical calculations are compared and summarized in Sec. IV, followed by discussions in Sec. V and conclusions in Sec. VI.

II. CHIRPED PHOTONIC CRYSTALS

A. Fabrication

The PhCs were fabricated in standard microscope soda-lime glass (Carl Roth, $n_{\mathrm{ref}} = 1.52$) by a point-by-point modification of refractive index by a tightly focused femtosecond laser beam. This method is widely used for inscription of various micro-optical and photonic components in glass, such as waveguides [13,14], Bragg gratings [15], as well as vortex generators [16]. The simplified schematic of the fabrication setup is depicted in Fig. 3(a). Due to high intensity of focused light, the refractive index at the region of the focal point is locally modified, thus translation of the sample results in a desired profile of modulation of refractive index in three dimensions. The change of refractive index and its spatial confinement depends on applied laser power. We used 300 fs pulse duration Yb:KGW laser providing 1030 nm wavelength radiation. The best results (the strongest refraction index modification) were obtained using 50 kHz repetition rate and 70 mW average power (before the objective, ∼13% of the power after passing it) 2.5 mm/s scanning speed, and 63 × 1.4 NA objective. This corresponds to 0.2 μJ energy per pulse 134 and 14 TW/cm^2 peak light intensity calculating as in [17] and assuming that voxel width is ∼500 nm for 1 μm transverse period. Further increase of irradiation power did not

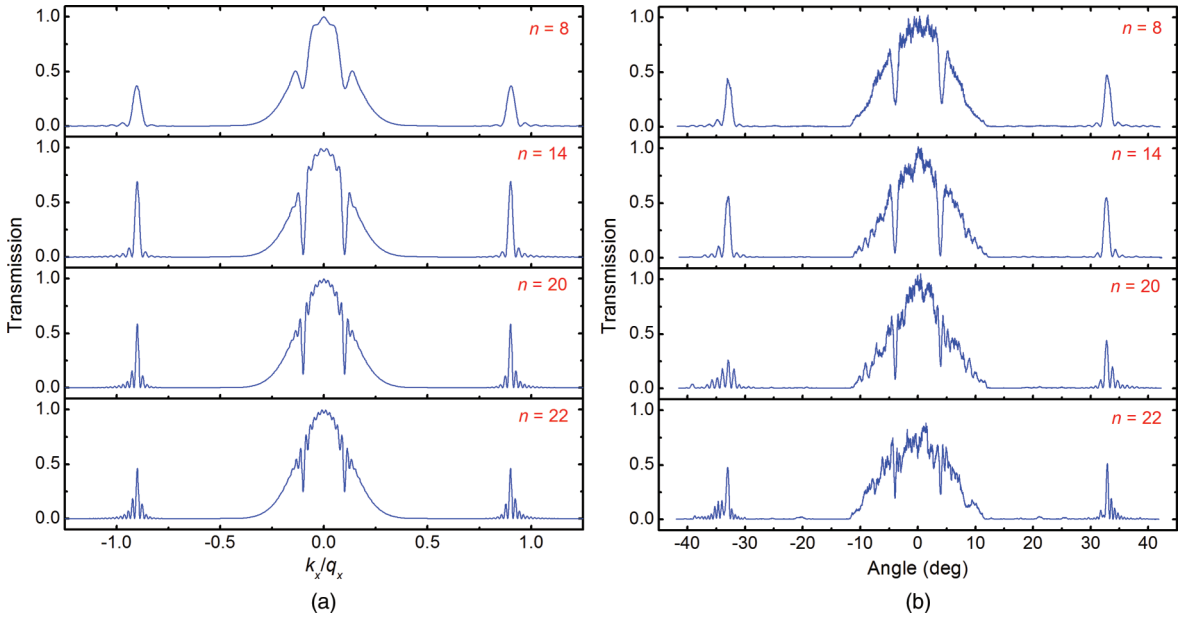

FIG. 2. (Color online) Angular profiles of filtered radiation depending on the length of the nonchirped PhCs (in terms of number of periods n). (a) Numerical and (b) experimental results. Details are provided in the main text.

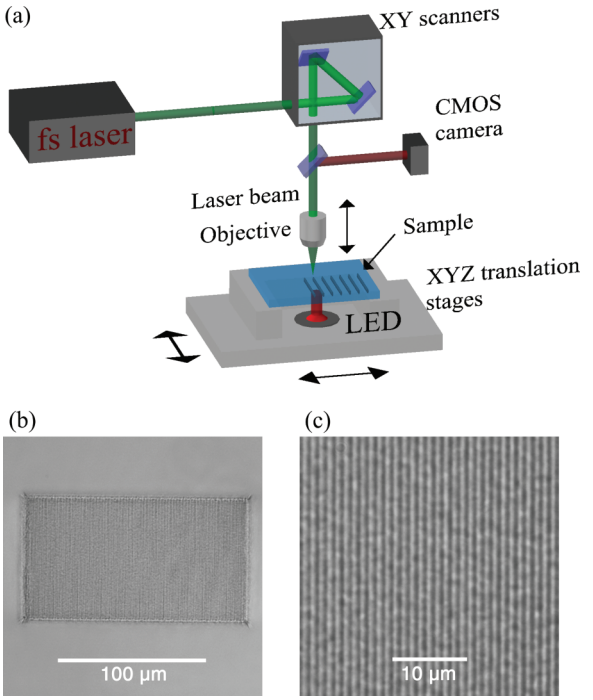

FIG. 3. (Color online) Fabrication setup and procedure (a). A sample of soda-lime glass is moved with respect to the tightly focused femtosecond pulse laser beam resulting in point-by-point refractive index modification in the bulk of the glass. (b) The optical microscopy image view and (c) the magnified image of the fabricated structure.

provide any significant increase in refractive index contrast, but introduced scattering defects, caused by distortion and thermal damage of affected regions.

B. Geometry

The PhCs were designed to have 100 layers of parallel, equally spaced rods with a 1 μm transverse period. Every second layer was shifted by half of the transverse period with respect to the previous one, thus two layers result in one longitudinal period. For chirped crystals the longitudinal period d_z is linearly incremented by Δd for every new period $d_{z,j} = d_{z,B} + j\Delta d$, where j counts the periods $i = 1,\ldots,n$. The adimensional chirp parameter is defined by $C = \Delta d/\overline{d_z}$, where $\overline{d_z} = (d_{z,\mathrm{Begin}} + d_{z,\mathrm{End}})/2$ is the average distance between layers. We chose $\overline{d_z}$ to be 6 μm and kept it constant in different samples, whereas the chirp parameter C was varied from sample to sample. Such fixed $\overline{d_z}$ corresponds to central filtering angle $\approx \pm 4$ deg.

C. Measurement

For measurements of filtering performance we illuminated the samples by continuous 633 nm wavelength HeNe laser beam focused into PhC samples with 10×0.3 NA objective (Fig. 4). Focusing provides a large angular range of the radiation illuminating the PhC. By measuring the angular intensity profile at the output of the PhC we determine which components are filtered out. To register the output a CCD camera was placed 3 cm behind the sample on a rotational stage, whose rotation axis is fixed at the focal point of the objective. Intensity profiles were recorded at different camera positions and combined, and far-field distribution was recorded and analyzed.

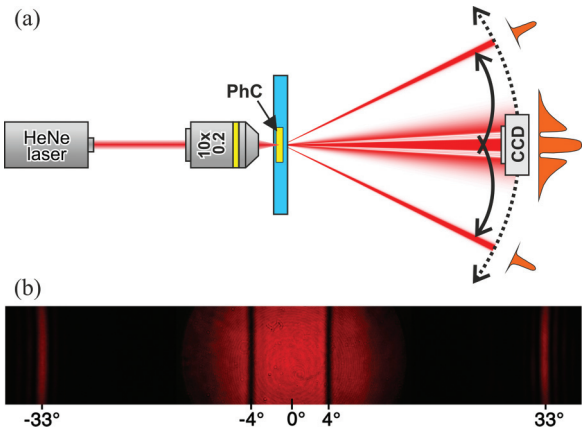

FIG. 4. (Color online) Experimental measurement scheme (a): The HeNe laser beam is focused into PhC. Part of the angular components is deflected to the diffraction maxima and the rest passes through. A CCD camera placed on the rotational stage measures the angular intensity profiles. (b) A part of CCD camera image of the beam behind the PhC (far field image).

III. NUMERICAL METHOD

We use a simplified version of the transfer matrix method, where we consider only the forward propagating wave components. A similar technique was used to calculate the field evolution in resonators filled by PhCs [18]. The transverse periodicity in lateral x direction imposes the transversal modulation of the field, therefore the field (at every longitudinal position z) can be Fourier expanded:

$$A(x,z) = e^{ik_x x}[a_0(z) + a_{-1}(z)e^{-iq_x x} + a_{+1}(z)e^{iq_x x} + a_{-2}(z)e^{-2iq_x x} + a_{+2}(z)e^{2iq_x x} + \cdots]. \quad (1)$$

The amplitudes of Fourier coefficients of the field expansion [equivalently the amplitudes of angular components with transverse wave numbers $(k_x + mq_x)$] constitute a column vector:

$$\vec{A}(z) = (\ldots,a_{-2},a_{-1},a_0,a_{+1},a_{+2},\ldots)^T. \quad (2)$$

Next we list consecutive field transformations along one full longitudinal period of the modulation of photonic structure.

A. Scattering by one layer

The periodical modulation in transverse direction couples the angular components of the field vector (2). In particular, the harmonic modulation couples only the neighboring field harmonics. We introduce phenomenological coupling coefficient s, which can be linked to microscopic parameters of the modulation of refraction index. The scattering matrix is

$$\hat{S} = \exp\begin{pmatrix} 0 & is & 0 & 0 & 0 \\ is & 0 & is & 0 & 0 \\ 0 & is & 0 & is & 0 \\ 0 & 0 & is & 0 & is \\ 0 & 0 & 0 & is & 0 \end{pmatrix}. \quad (3)$$

For a more simple presentation we consider the scattering truncated to five harmonic components.

B. Free propagation

The free propagation between the scattering layers is considered by the paraxial propagation equation:

$$\partial_z A(x,z) = \frac{i}{2k_0}\frac{\partial^2}{\partial x^2}A(x,z). \tag{4}$$

Substitution of expansion (1) into (4) yields the equation system:

$$d_z a_m(z) = -\frac{i}{2k_0}(mq_x + k_x)^2 a_m(z). \tag{5}$$

The integration of (5) over half of a longitudinal period results in diagonal field transformation matrix:

$$\hat{P} = e^{-iLk_x^2/2}\cdot \mathrm{Diag}\big(e^{-iL(k_x-2q_x)^2}, e^{-iL(k_x-q_x)^2}, e^{-iLk_x^2}, e^{-iL(k_x+q_x)^2}, e^{-iL(k_x+2q_x)^2}\big). \tag{6}$$

Here $L = d_z/(2k_0)$ is the normalized longitudinal period.

C. Lateral shift of the grating

Every second scattering layer is laterally shifted by half of the transverse period. We account for this lateral shift using the following trick. We fix the reference frame with the position of the first grating. Then, for the calculation of the scattering from the laterally shifted grating, we change the reference frame by applying the field transformation operator:

$$\hat{M} = \mathrm{Diag}(e^{-2im_x q_x}, e^{-im_x q_x}, 1, e^{+im_x q_x}, e^{+2im_x q_x}). \tag{7}$$

In the following, after calculation the scattering by the second scattering layer [by using (3) in the new reference frame], we restore the original reference frame, by applying $\hat{M}^{-1}$.

D. Full period

The field transformation along the full longitudinal period is calculated by applying consecutively (from right to left) all the operators presented above:

$$\hat{T}_i = \hat{P}\hat{M}^{-1}\hat{S}\hat{M}\hat{P}\hat{S}. \tag{8}$$

For the chirped crystal the parameters of one period transfer matrix depend on the lattice parameters in the concrete period. The full transmission matrix is a matrix product of (8): $\hat{T} = \prod_i \hat{T}_i$. The transmission of the central component is given by the central element $T_{0,0}$ of the full transmission matrix $\hat{T}$. The scattering into sidebands harmonics is described by the corresponding off-diagonal column elements of the matrix, e.g., by elements $T_{-1,0}$ and $T_{+1,0}$ for scattering into first diffraction components.

The coupling coefficient s depends on the modulation amplitude of the refractive index, which is of order of $\Delta n \sim 10^{-3}$, the precise value of which is, however, unknown. We determined the value of s by calibrating the experimental data with numerical calculation results for light propagation through unchirped crystal (see Fig. 2). For our samples the s has been estimated $s \approx 0.05$, which means that approximately $s^2 = 0.25\%$ of radiation diffracts in every layer. We note that this calibration allowed us to estimate the variation of refraction index of the sample, which comes out to be approximately $\Delta n \approx 3 \times 10^{-3}$ for our samples fabricated with optimum parameters.

IV. SUMMARY OF THE RESULTS

The main results of the study are summarized in Fig. 5, which evidences the constructive role of the chirp for spatial filtering performance. The angular range as well as the energy of filtered-out radiation increases with increasing chirp as expected. The experimental results correspond qualitatively

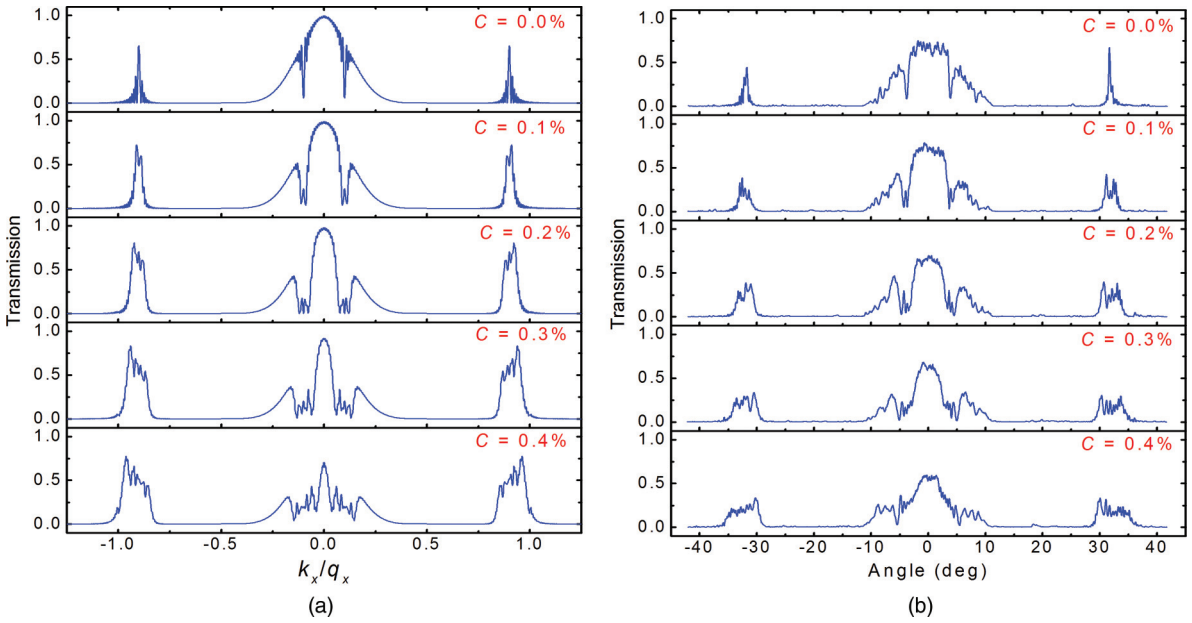

FIG. 5. (Color online) Angular transmission profiles for varying chirp parameter C for PhC sample with $n = 50$ periods. (a) Numerical and (b) experimental results. Transverse wave number k_x is normalized to transverse wave number of refractive index modulation q_x in (a).

well to the numerical calculation results. Some discrepancy between the experimental measurements and numerical results appears, especially for large values of the chirp, which is due to imperfections of fabrication of the samples. Overall, although the measured efficiency of the filtering increases with increasing chirp parameter, the increase is, however, slower than that following from numerical calculations. Our interpretation is that for larger chirp parameters the filtered areas become more broad and "shallow" (for a fixed length of the sample) and generally they "collect" more noise due to the imperfections of the structure. We note, however, that the detailed analysis of the randomness of structure requires separate analysis, and is beyond the scope of the present study.

Next we calculate quantitative data of the filtering performance. We define filtering performance by

$$F = \frac{\int |\Delta I(k_x)| dk_x}{\int |I(k_x)| dk_x}, \tag{9}$$

which has a meaning of depletion of energy normalized to the full energy. The integration in (9) is performed over the Brillouin zone, i.e., on interval $k_x \in [-q_x/2, q_x/2]$. For proper geometry, when precisely the wings from the angular spectra are filtered out, the F is a measure of relative narrowing of the angular spectrum.

Figure 6(a) summarizes the dependence of the filtering performance on the chirp parameter. If the filtering in unchirped PhC structures of increasing length saturates for short crystals ($n = 15$ periods), then for chirped crystals the saturation begins for longer crystals and results in higher filtering performance values, correspondingly. Figure 6(b) shows the dependence of filtering on the length of the sample for different chirp parameters C.

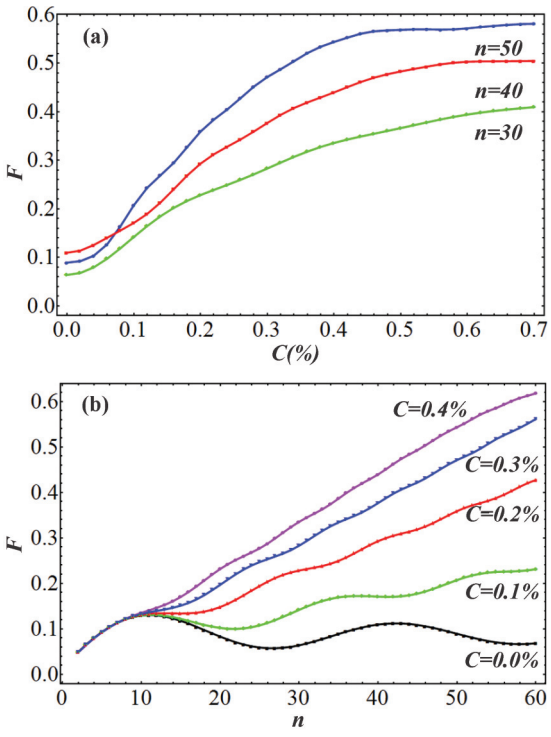

FIG. 6. (Color online) Numerical study of the filtering performance: (a) dependences of filtering efficiency on chirp parameter for several crystals of different length (green plot for $n = 30$, red for $n = 40$, blue for $n = 50$); (b) Dependences of filtering efficiency on number of periods with different chirp parameters (black plot for $C = 0.0\%$; green for $C = 0.1\%$, red for $C = 0.2\%$, blue for $C = 0.3\%$, violet for $C = 0.4\%$).

V. DISCUSSIONS

The above theoretical study is performed with the parameters corresponding to fabricated structures: The values of the coupling were $s = 0.05$ which correspond to the maximum achievable coupling for structures imprinted in glass. We also restricted to realistic length of the PhC, possible to write without large distortions, which is approximately $n = 60$ periods. With the increasing length of the structure the imperfections of fabrication, as well as the losses and scattering of the structure, increase. However, even with these restrictions the filtering performance close to approximately 50% has been experimentally demonstrated.

Looking into perspective, we analyzed the filtering performance of "hypothetical PhCs" with larger refraction index modulation, i.e., with corresponding larger coupling parameters s than those possible to obtain in reality for PhCs build in glasses. Examples of calculations for longer and higher index contrast photonic structures are shown in Fig. 7. Both calculated cases show that the filtering performance can reach the values of 80%, and could result in impressive enhancement of the beam quality by factor of 3.

The filtering performance depending on parameters s, n, and C is summarized in Fig 8. As follows from Figs. 8(a) and 8(c) the chirp parameter C has optimum values, which depends on the coupling parameter s: stronger coupling results in shorter filtering saturation length, therefore requires larger chirp for maximum filtering performances. The dependence of filtering performance on the length of PhC, as follows from Figs. 8(b) and 8(d), shows the monotonic increase with eventual saturation.

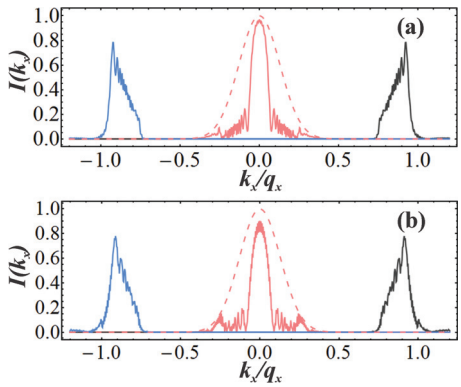

FIG. 7. (Color online) Numerically obtained field profiles for spatial filtering in chirped structures with higher number of periods (a) and for higher refraction index contrast (b). The parameters for (a): $n = 120$, $s = 0.05$, $C = 0.24\%$, $d_z = 7.44\ \mu$m; for (b): $s = 0.1$, $n = 50$, $C = 0.53\%$, $d_z = 7.2\ \mu$m. The dashed line indicates angular profile of incident beam.

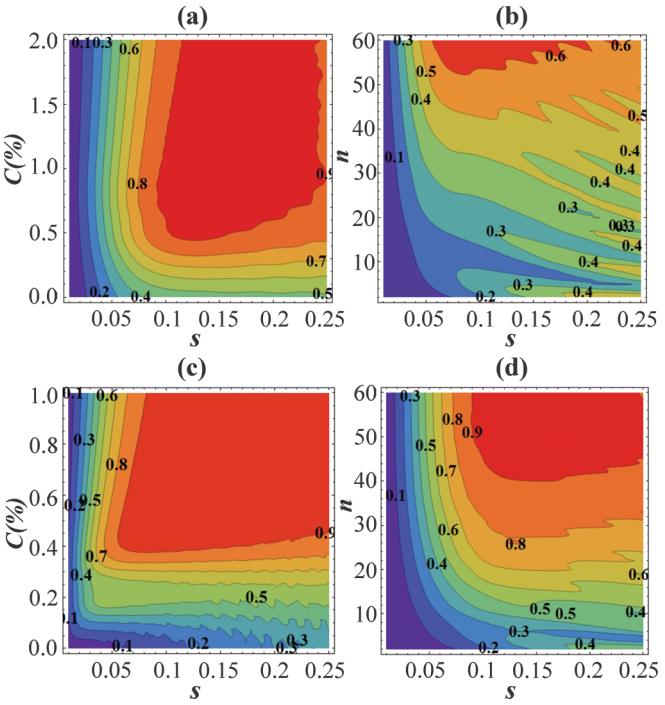

FIG. 8. (Color online) The filtering efficiency, represented by isolines and by different colors, depending on sets of parameters. (a), (c) show dependencies on C and s; (b), (d) show dependencies on n and s. Parameters: (a) $n = 50$, (c) $n = 120$. (b) $C = 0.3\%$, and (d) $C = 1\%$.

VI. CONCLUSIONS

In conclusion, we have theoretically calculated and experimentally proved the effect of chirping of photonic crystal on the efficiency of spatial filtering. Our theoretical-numerical analysis reproduces well the experimental observations and interprets the observed effect as the spatial filtering in the gapless configuration.

In spite of relatively weak index modulation (small scattering by one row) a substantial part of the radiation was shown to be filtered out. In order to obtain a technologically utile spatial filter the higher (but moderate) index contrast PhCs are necessary, which are to be based on new materials and fabrication technologies. A technologically relevant spatial filtering, allowing us to improve the beam quality parameter by the factor of 2–3, requires the refractive index modulation of order of approximately $\Delta n_0 = 10^{-2}$.

Finally we highlight the advantage of the method of filtering demonstrated in the present article. The main advantages (comparing with the conventional pinhole spatial filer) are: (1) extremely small thickness (hundreds of microns) of the filter enabling the integration of such a filter into micro-optical devices or into microresonators of small lasers; (2) translational invariance of the PhC spatial filter (insensitivity to the lateral shift of PhC structure) simplifying its utilization; and (3) possibility to combine (to add) the filtering functionality to some other, already existing, functionalities (amplification, nonlinearities) in bulk material, by additional modulation of refraction index of the (amplifying or nonlinear) material.

ACKNOWLEDGMENTS

We acknowledge financial support by Spanish Ministerio de Educación y Ciencia and European FEDER (project FIS2011-29734-C02-01), Generalitat de Catalunya (2009 SGR 1168), and "Mikrošviesa" (No. MIP-12241) from the Research Council of Lithuania. M. Peckus acknowledges his postdoctoral fellowship funded by European Union Structural Funds project "Postdoctoral Fellowship Implementation in Lithuania".

[1] A. E. Siegman, Proc. SPIE **1868**, 2 (1993).
[2] E. Yablonovitch, Phys. Rev. Lett. **58**, 2059 (1987).
[3] A. E. Serebryannikov *et al.*, Appl. Phys. Lett. **94**, 181101 (2009).
[4] Evrim Colak *et al.*, J. Appl. Phys. **108**, 113106 (2010).
[5] I. Moreno *et al.*, Opt. Lett. **30**, 914 (2005).
[6] Z. Luo *et al.*, Appl. Phys. B **94**, 641 (2009).
[7] Z. Tang *et al.*, Chin. Opt. Lett. **5**, S211 (2007).
[8] V. J. Sánchez-Morcillo *et al.*, Appl. Acoust. **73**, 302 (2012).
[9] R. Pico *et al.*, Appl. Acoust. **74**, 945 (2013).
[10] K. Staliunas and V. J. Sánchez-Morcillo, Phys. Rev. A **79**, 053807 (2009).
[11] L. Maigyte *et al.*, Phys. Rev. A **82**, 043819 (2010).
[12] K. Staliunas, Phys. Rev. A **84**, 013626 (2011).
[13] K. M. Davis *et al.*, Opt. Lett. **21**, 21 (1996).
[14] S. Nolte *et al.*, Appl. Phys. A **77**, 109 (2003).
[15] H. Zhang *et al.*, Opt. Lett. **32**, 2559 (2007).
[16] M. Beresna *et al.*, Appl. Phys. Lett. **98**, 201101 (2011).
[17] M. Malinauskas *et al.*, Opt. Express **19**, 5602 (2011).
[18] M. Peckus *et al.*, Phys. Rev. A **79**, 033806 (2009).